Stem Cell Reports
Article

ISSCR

OPEN ACCESS

Electrophysiologic Characterization of Calcium Handling in Human Induced Pluripotent Stem Cell-Derived Atrial Cardiomyocytes

Mariana Argenziano,[1,2,5] Erin Lambers,[1,5] Liang Hong,[1] Arvind Sridhar,[1] Meihong Zhang,[1] Brandon Chalazan,[1] Ambili Menon,[1] Eleonora Savio-Galimberti,[1,2] Joseph C. Wu,[3] Jalees Rehman,[1,4] and Dawood Darbar[1,4,*]

[1]Division of Cardiology, Department of Medicine, University of Illinois at Chicago, 840 S. Wood Street, 920S (MC 715), Chicago, IL 60612, USA
[2]Lankenau Institute for Medical Research, Wynnewood, PA, USA
[3]Division of Cardiology, Department of Medicine, Stanford Cardiovascular Institute, Stanford University Medical Center, Stanford, CA, USA
[4]Department of Pharmacology, University of Illinois at Chicago, Chicago, IL, USA
[5]Co-first author
*Correspondence: darbar@uic.edu
https://doi.org/10.1016/j.stemcr.2018.04.005

SUMMARY

Human induced pluripotent stem cell (hiPSC)-derived atrial cardiomyocytes (CMs) hold great promise for elucidating underlying cellular mechanisms that cause atrial fibrillation (AF). In order to use atrial-like hiPSC-CMs for arrhythmia modeling, it is essential to better understand the molecular and electrophysiological phenotype of these cells. We performed comprehensive molecular, transcriptomic, and electrophysiologic analyses of retinoic acid (RA)-guided hiPSC atrial-like CMs and demonstrate that RA results in differential expression of genes involved in calcium ion homeostasis that directly interact with an RA receptor, chicken ovalbumin upstream promoter-transcription factor 2 (COUP-TFII). We report a mechanism by which RA generates an atrial-like electrophysiologic signature through the downstream regulation of calcium channel gene expression by COUP-TFII and modulation of calcium handling. Collectively, our results provide important insights into the underlying molecular mechanisms that regulate atrial-like hiPSC-CM electrophysiology and support the use of atrial-like CMs derived from hiPSCs to model AF.

INTRODUCTION

The generation of human induced pluripotent stem cell-derived cardiomyocytes (hiPSC-CMs) from peripheral blood mononuclear cells has provided insights into underlying cellular mechanisms of inherited arrhythmia syndromes such as catecholaminergic polymorphic ventricular tachycardia, Brugada syndrome, and long QT syndrome (Shi et al., 2017; Liang et al., 2016). Ventricular-like hiPSC-CMs are increasingly being used to model ventricular arrhythmia syndromes (Itzhaki et al., 2011, 2012; Liang et al., 2016; Chugh et al., 2014). However, less is known about the potential role of atrial-like hiPSC-CMs to model atrial arrhythmias such as atrial fibrillation (AF), which is the most prevalent and clinically significant arrhythmia in adults (Patel et al., 2014).

Currently, one of the main strategies to differentiate hiPSCs to CMs is by replicating endogenous signaling pathways important for mammalian heart development (Liang and Zhang, 2013). Several groups have reported the use of growth factors and small molecules to improve reproducibility and efficiency of hiPSC-CM differentiation and maturation. However, patient-specific iPSC-CMs exhibit a highly heterogeneous population of atrial-, nodal-, and ventricular-like cells (Mummery et al., 2012). Furthermore, the molecular and electrophysiological properties of hiPSC-CMs differ considerably when compared with human CMs and differentiation toward the atrial phenotype remains a major challenge. A recent study (Devalla et al., 2015) generated atrial-like CMs derived from human embryonic stem cells (hESCs) by modulating the retinoic acid (RA) signaling pathway to model pre-clinical testing of atrial-specific antiarrhythmic drugs (AADs). With the upregulation of several atrial-specific markers and action potential (AP) morphology that was similar to that of neonatal human atrial CMs, RA directed hESC-CMs into a more atrial-like phenotype. Molecular characterization of the intermediate progenitors generated during the differentiation of hPSCs (Lee et al., 2017) showed that differentiation of human atrial and ventricular CMs mandates not only distinct mesodermal populations but also patterning that is regulated by an autocrine RA signaling pathway. However, the electrophysiological phenotype of atrial-like hiPSC-CMS is not fully understood, and, in order to use atrial-like CMs for arrhythmia modeling or assessing AAD responses, it is essential to better understand the electrophysiological phenotype of these cells.

The purpose of this study was to comprehensively evaluate the molecular, transcriptomic, and electrophysiologic mechanisms that mediate RA-guided hiPSC atrial-like CMs. We show that a combined approach of RA with glucose starvation and monolayer culturing not only increases hiPSC-CM commitment into a more atrial-like phenotype but also results in differential expression of genes involved in calcium ion homeostasis that directly interact with an RA receptor, chicken ovalbumin upstream

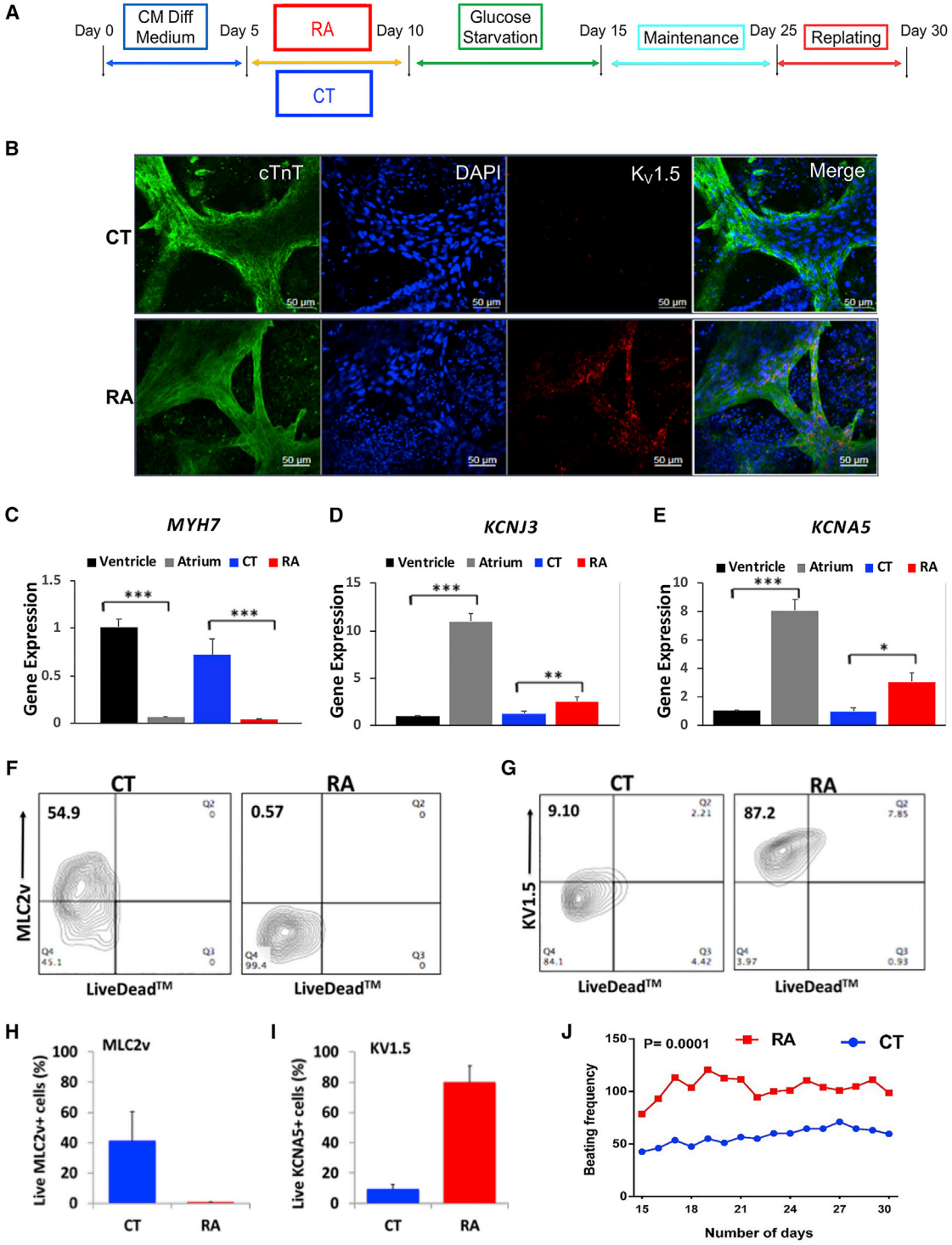

Figure 1. RA-Guided Differentiation of hiPSC-CMs Results in Increased Beating Frequency

(A) Protocol for cardiac differentiation after small molecule differentiation; cells are incubated in 1 µM RA or DMSO for 5 days. At day 10, cells are enriched by glucose starvation. Analysis is performed at days 10, 15, and 30. Diff, differentiation.

(B) Immunostaining showing the protein expression of pan-CM marker cardiac cTnT and atrial marker Kv1.5 in hiPSC-CMs at day 10.

(C) qRT-PCR of ventricular markers, *MYH7*, in RA-treated and CT cells.

(D and E) qRT-PCR of atrial markers *KCNJ3* (D) and *KCNA5* (E) in RA-treated and CT cells at day 30.

(legend continued on next page)

promoter-transcription factor 2 (COUP-TFII). In line with molecular assessments, we further demonstrate that RA modulates calcium uptake and release as well as L-type calcium current ($I_{Ca,L}$). We report for the first time a mechanism by which RA generates an atrial-like electrophysiologic signature through the downstream regulation of calcium channel gene expression by COUP-TFII and modulation of calcium handling. Collectively, our results provide important insights into the underlying molecular mechanisms that regulate atrial-like hiPSC-CM electrophysiology and support the use of atrial-like CMs derived from hiPSCs to model AF.

RESULTS

RA-Guided Differentiation of hiPSC-CMs Results in Increased Beating Frequency

We differentiated two independently derived control (CT) hiPSCs (L1 and L2) that exhibited a normal karyotype and pluripotency profile (Figure S1) for 5 days followed by treatment with RA for 5 days with daily media changes. Between days 10 and 15, iPSC-CMs were enriched using the glucose starvation selection method (Sharma et al., 2015) where glucose is replaced by lactate and replated after 5 days (Figure 1A). Immunofluorescence staining of cardiac troponin T (cTnT), a pan-CM marker, showed similar expression levels between groups, while $K_V1.5$, an atrial-specific marker, expression was much higher in RA-treated compared with CT (DMSO)-treated cells at day 10 of differentiation (Figure 1B). To analyze the specific types of CMs generated from RA-treated versus CT cells, we examined relative gene expression levels of atrial and ventricular CM markers. Real-time qPCR revealed that RA-treated hiPSC-CMs compared with CT exhibit decreased gene expression of the ventricular marker *MYH7* (Figure 1C) as well as increased expression of atrial markers *KCNJ3* and *KCNA5* (Figures 1D and 1E). These expression patterns were similar to those seen in adult human atrial and ventricular tissue, thus supporting the validity of the atrial differentiation approach in hiPSCs (Figures 1C–1E). We then examined the percentage of cells expressing the ventricular marker MLC2v and the atrial marker Kv1.5. Flow cytometry revealed a significant decrease in the percentage of cells expressing MLC2v in RA-treated cells (0.84% ± 0.2%) compared with CT cells (41.4% ± 19.1%; $p < 0.05$; Figures 1F and 1H). It also demonstrated a significant increase in the percentage of cells expressing Kv1.5 in RA-treated cells (80.2% ± 10.5%) compared with CT cells (9.6% ± 2.8%; $p < 0.001$; Figures 1G and 1I). These data indicate that RA treatment during days 5–10 of differentiation results in the enrichment of atrial-like CMs. RA-treated cells also had a higher beating frequency, which may be reflective of a nodal phenotype (Figure 1J).

Transcriptomic and Chromatin Immunoprecipitation Analysis of RA- and CT-Treated hiPSC-CMs Reveal Differential Expression of Calcium Channel Genes Associated with COUPTF-II Protein

We examined the transcriptional landscape of hiPSC-CMs treated with RA versus CT cells to identify differentially regulated gene pathways that may explain the enrichment and electrophysiologic phenotype of atrial-like hiPSC-CMs. Transcriptomic analysis of CT and RA-treated hiPSC-CMs was performed at day 30. Hierarchical clustering of differential expression genes (DEGs) in CT and RA hiPSC-CMs showed two main clusters with samples of the same group clustered together (Figure 2A). A total of 159 DEGs were identified with 106 upregulated and 53 downregulated (Figure 2B). Gene Ontology (GO) pathway analyses of the DEGs identified both up- and downregulated pathways in RA-treated versus CT hiPSC-CMs. The upregulated pathways included those involving atrial development, sino-atrial node (SAN) AP, cardiac conduction regulation of heart rate, and cardiac muscle contraction (Table S1). Downregulated pathways included those involved with development of ventricular tissue, ventricular cardiac muscle cell AP, and calcium ion import into the sarcoplasmic reticulum, and regulation of cardiac muscle contraction by calcium ion signaling (Table S1). Ventricular genes were significantly downregulated (*MYL2*, *MYH7*), while atrial genes were upregulated (*NR2F2*, *KCNJ3*, *GJA5*; Figure 2C). We also found that *CACNA1C* and *CACNA1G* were differentially expressed (Figures 2C–2F), while *SERCA2* and *RyR2*, important for calcium ion homeostasis, remained unchanged (Figures 2D–2F). Regulation of

(F) Representative flow cytometry contour plots of RA-treated and CT cells sorted into MLC2v positive and live fractions at day 10 (quadrant 1, upper left).

(G) Representative flow cytometry contour plots of RA-treated and CT cells sorted into Kv1.5 positive and live fractions at day 10 (quadrant 1, upper left).

(H and I) Averaged flow cytometry data from three biological replicates for live MLC2v (H) and Kv1.5 (I) flow cytometry fractions, respectively.

(J) Comparison of beating frequency measured on hiPSC-CMs from CT and RA groups days 15–30.

Data shown in all panels represent three pooled independent biological experiments displayed as mean ± SD, n = 3; *$p < 0.05$, **$p < 0.01$, ***$p < 0.001$.

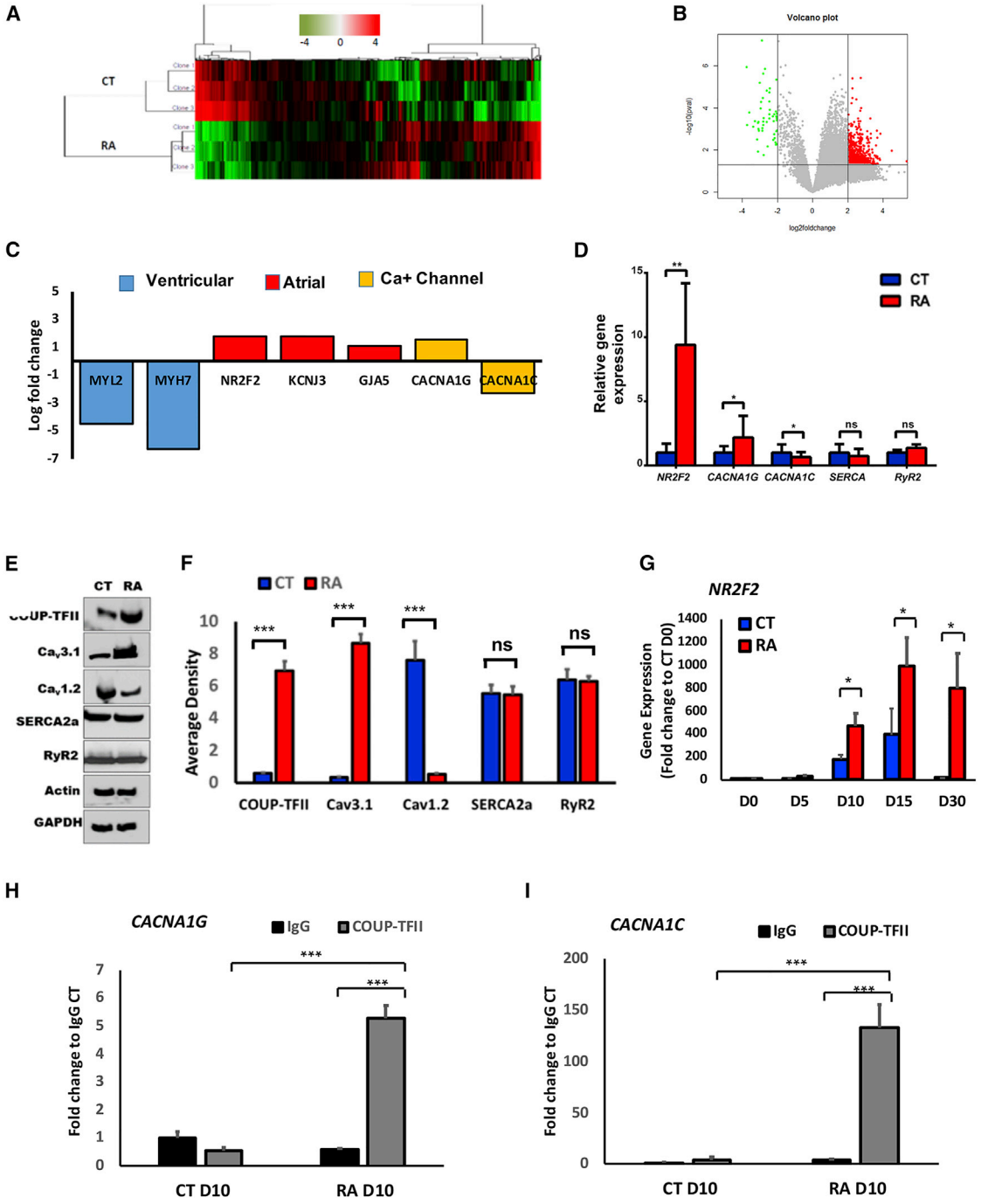

Figure 2. Transcriptomic and ChIP Analysis of RA-Treated and CT hiPSC-CMs Reveal Differential Expression of Calcium Channel Genes Associated with COUP-TFII

(A) Hierarchical clustering of DEGs in CT and RA hiPSC-CMs.

(B) Volcano plot of RA-treated hiPSC-CMs (red) and CT (green) showing DEG with an absolute log2 of fold change >2 (x axis) and $p < 0.05$ (y axis).

(C) Bar graph showing log2 fold change RPKM (reads per kilobase of coding sequence per million mapped) of RA-treated hiPSC-CMs relative to CT hiPSC-CMs. Levels of ventricular, atrial, nodal, and Ca channel genes were significantly differentially expressed with $p < 0.05$.

(D) Real-time qPCR of *NR2F2*, *CACNA1G*, and *CACNA1C*, *SERCA*, and *RyR2* in RA-treated and CT cells.

(E) Representative western blots showing protein expression levels of COUP-TFII, Cav3.1, and Cav1.2, SERCA2A, and RyR2.

(F) Densitometry analysis of COUP-TFII, HCN4, Cav3.1, and Cav1.2.

(legend continued on next page)

these genes downstream of RA could be responsible for the functional differences we observed in RA-treated versus CT cells, including increased beating frequency.

Our data show that nuclear receptor subfamily 2, group F, member 2 (*NR2F2*) expression is highly upregulated in RA-treated versus CT cells (Figures 2C–2F). *NR2F2* encodes a transcription factor, COUP-TFII, that regulates atrial development and identity (Pereira et al., 1999). A prior study reported involvement of COUP-TFII in RA signaling as a downstream receptor of RA (Devalla et al., 2015). A more recent study has shown that COUP-TFII can serve as a dual marker for atrial CMs along with NKX2-5, although is not necessary for atrial-like lineage specification (Schwach et al., 2017). Therefore, we hypothesized that COUP-TFII may function in parallel with other lineage specification pathways to modulate selected gene pathways important for the functional maturation of atrial-like cells through regulation of DEGs shown in Figure 2C. Using the University of California Santa Cruz genome browser (https://genome.ucsc.edu/ENCODE/) to explore transcription factor chromatin immunoprecipitation sequencing (ChIP-seq) analysis (Landt et al., 2012), we identified two calcium channel genes associated with the COUP-TFII protein: (1) *CACNA1G* encodes the T-type calcium channel expressed in pacemaker cells (Figure S2A), and (2) *CACNA1C* encodes the voltage-gated L-type calcium channel (Figure S2B). Additionally, the genomic locations where COUP-TFII binds to *CACNA1G* and *CACNA1C* in human atrial cells and CMs are sensitive to DNase treatment, indicating that they are accessible for transcriptional regulation and are also highly conserved across species (Figures S2A and S2B). Next, we validated the association between COUP-TFII and *CACNA1G* and *CACNA1C* binding sites in RA-treated and CT hiPSC-CMs at day 10 of differentiation when COUPTF-II is first significantly expressed (Figure 2G). COUP-TFII binding to the promoters of *CACNA1G* (Figure 2H) and *CACNA1C* (Figure 2I) was significantly increased in RA versus CT hiPSCs. Collectively, these data indicate that COUP-TFII may bind to *CACNA1G* and *CACNA1C*, thereby regulating their gene expression and modulating calcium handling in atrial-like hiPSC-CMs.

Electrophysiologic Characterization Reveals RA Treatment Increases Atrial- and Nodal-like Cell AP Morphologies

To use atrial-like CMs for disease modeling it is essential to assess the electrophysiologic phenotypes of the cells. AP recordings using sharp microelectrodes in monolayers revealed three morphologies (Figure 3A). Ventricular, atrial, and nodal APs were classified according to published criteria (Ma et al., 2011). Ventricular-like APs had a ratio (APD30 [AP duration at 30% repolarization]–APD40/APD70–80) ~1 compared with the atrial-like ratio of ~0.5. In RA-treated cells nodal- (6%), atrial- (85%), and ventricular-like (9%) hiPSC-CMs were observed (Figure 3B). In contrast, in CT cells, mostly APs with ventricular morphology were observed (86%) with low yield of nodal- (7%) and atrial-like (7%) hiPSC-CMs (Figure 3B). Atrial- and ventricular-like hiPSC-CMs displayed similar resting membrane potentials (RMPs), AP amplitude (APA) was larger in CT cells (63.9 ± 1.9 versus 50.9 ± 4.0 mV, $p < 0.05$), and the beating frequency was increased in the RA group (2.5 ± 0.1 versus 1.2 ± 0.04 Hz, $p < 0.0001$). APD was shorter in RA-treated hiPSC-CMs (Table 1). Similar results were found in the second independently derived hiPSC-L1 (Figure S3). Collectively, these data support the hypothesis that RA treatment of hiPSCs results in the electrophysiologic phenotype of atrial-like cells in part through the modulation of calcium handling proteins.

RA Treatment Increases Atrial-Specific $I_{K,ACh}$ in Response to Carbachol and Adenosine

To characterize atrial-specific currents in RA-treated cells, we examined $I_{K,ACh}$, encoded by *KCNJ3/KCNJ5*, in RA-treated versus CT hiPSC-L1-CMs. A carbachol (10 μM) sensitive current was recorded in RA-treated hiPSC-CMs but absent in CT hiPSC-CMs (Figures 3D and 3E). Similar results were found for hiPSC-L2-CMs (Figures S3C–S3E). We also examined a second atrial-specific current activated by adenosine. An adenosine-activated potassium current was recorded in RA-treated versus CT hiPSCs (Figures 3F–3H and S3). Collectively, these data demonstrate that RA-treated hiPSC-CMs possess a more atrial-like electrophysiologic signature compared with CT hiPSC-CMs.

RA Treatment Increases Rate of Calcium Uptake and Release in Atrial-like hiPSC-CMs

We measured spontaneous calcium transients in RA-treated versus CT cells derived from hiPSC-L1 (Figure 4A). Calcium transients were obtained using confocal microscopy and Fluo-4-AM (4-(6-acetoxymethoxy-2,7-difluoro-3-oxo-9-xanthenyl)-4′-methyl-2,2′-(ethylenedioxy)dianiline-N,N,N′,N′-tetraacetic acid tetrakis(acetoxymethyl) ester) loaded cells. Measurements were performed at

(G–I) NR2F2 gene expression throughout the differentiation of hiPSC-L1-CMs (G). (H) ChIP-qPCR showing enrichment of *CACNA1G* and (I) *CACNA1C* followed by immunoprecipitation of COUP-TFII in RA-treated and CT hiPSC-L1-CMs at day 10 of differentiation. IgG, immunoglobulin G.

Data shown in all panels represent three pooled independent biological experiments displayed as mean ± SD, n = 3; *$p < 0.05$, **$p < 0.01$, ***$p < 0.001$.

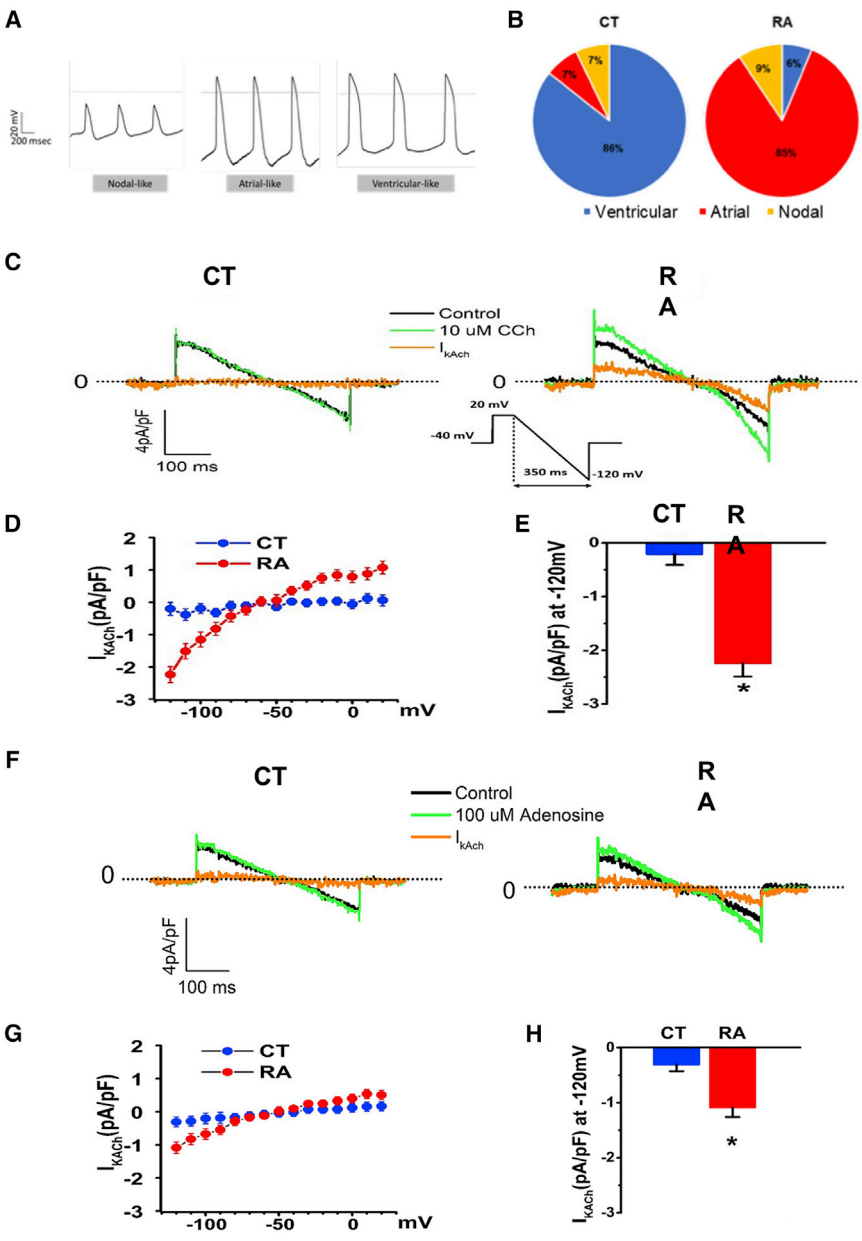

Figure 3. RA Treatment Increases Proportion of Atrial-like AP Morphologies and Atrial-Specific $I_{K,ACh}$ Response to Carbachol and Adenosine

(A) Representative images of three major types of AP morphologies observed in hiPSC-L1-CMs: atrial-, nodal-, and ventricular-like. AP morphologies were recorded using intracellular sharp microelectrode recordings of single cells within monolayers.

(B) Pie graphs displaying the percentage of morphologies observed in RA-treated (n = 32 cells) and CT hiPSC-L1-CMs (n = 42 cells).

(C) Representative recordings of 10 μM carbachol (Cch) sensitive current ($I_{K,ACh}$) in ventricular-like (CT) and atrial-like CMs (RA); voltage protocol is shown in inset.

(D) Current-voltage relationship (I-V curve) for Cch sensitive $I_{K,ACh}$ densities in ventricular-like and atrial-like CMs; n = 3 cells each group.

(E) Quantification of $I_{K,ACh}$ densities at −120 mV in ventricular-like and atrial-like CMs; n = 3 cells each group.

(F) Representative recordings of 100 μM adenosine sensitive current ($I_{K,ACh}$) in ventricular-like (CT) and atrial-like CMs (RA).

(G) Current-voltage relationship (I-V curve) for adenosine sensitive $I_{K,ACh}$ densities in ventricular-like and atrial-like CMs; n = 4 cells each group.

(H) Quantification of $I_{K,ACh}$ densities at −120 mV in ventricular-like and atrial-like CMs; n = 4 cells each group.

Data shown in all panels represent pooled independent biological experiments displayed as mean ± SD, *p < 0.05.

room temperature. Representative line scans show spontaneous calcium release events (sCaREs) recorded from CT and RA-treated cells (Figure 4B). Superimposed calcium transients from CT and RA-treated hiPSC-CMs showed smaller amplitude for the RA-treated cells (Figure 4C) and a shorter transient when normalized (Figure 4D). Calcium transient traces obtained from RA-treated cells showed a shorter cycle length (407.3 ± 10.6 versus 875.0 ± 50.8 ms, n = 25, $p < 0.001$; Figure 4E) with a decreased peak F/F_o (1.21 ± 0.10 versus 2.36 ± 0.19 ms, n = 25, $p < 0.001$; Figure 4F) when compared with CT cells. Normalized transients from RA-treated cells have a similar slope value (34.8 ± 3.7 versus 35.7 ± 4.8 F/Fo ms^{-1}, n = 25; Figure 4G) with a shorter duration (278.7 ± 14.4 versus 583.8 ± 31.5 ms, n = 25, $p < 0.001$; Figure 4H) and shorter time to peak (TTP; 37.7 ± 2.7 versus 78.6 ± 4.7 ms, n = 25, $p < 0.001$, Figure 4I). The results were comparable when measured in hiPSC-L2-CMs (Figures S3F–S3K). These data indicate that RA treatment has a significant impact on calcium transients in atrial-like hiPSC-CMs with a shorter duration of cycle length, due to higher spontaneous beating frequency and reduced peak amplitude, slope, and TTP. These data represent an electrophysiologic signature for calcium handling in RA-treated hiPSC-CMs.

Table 1. Electrophysiological Parameters of Spontaneously Beating hiPSC-L1-CMs Treated with RA versus CT

AP Parameter	CT	RA	p Value
n	42	32	
RMP (mV)	−43.2 ± 1.5	−45.2 ± 2.7	ns
APA (mV)	63.9 ± 1.9	50.9 ± 4.0	<0.05
APD50 (ms)	126.3 ± 6.8	57.5 ± 2.7	<0.01
APD90 (ms)	218.1 ± 14.0	89.0 ± 4.5	<0.001
APD90/APD50 (ratio)	1.7 ± 0.06	1.3 ± 0.01	<0.01
APD30–40/APD70–80	0.97 ± 0.12	0.48 ± 0.03	<0.01
Upstroke velocity (V/s)	29.3 ± 2.7	22.5 ± 5.3	ns

AP, action potential; APA, AP amplitude; APD50, AP duration at 50% repolarization; APD90, AP duration at 90% repolarization; CT, control (DMSO); ns, not significant.

RA Treatment Reduces Calcium Channel Currents and Limits Availability

We recorded the voltage-gated $I_{Ca,L}$ in RA-treated versus CT hiPSC-CMs with single-cell patch-clamp techniques. We observed that the peak $I_{Ca,L}$ amplitude (Figure 4L) and current density (Figure 4M) were significantly reduced in RA-treated cells when compared with CT cells during the process of voltage-dependent activation (Figure 4K). We then determined the conductance-voltage relationship (G-V curve) of RA-treated versus CT hiPSC-CMs, and showed that the curve for RA-treated cells was shifted to the right (depolarizing) compared with CT, indicating reduced channel availability (Figure 4N). This finding is consistent with previous reports in adult rat atria versus ventricle (Hatano et al., 2006) and may represent an electrophysiologic feature of calcium currents in atrial-like hiPSC-CMs.

DISCUSSION

There is a fundamental gap in our understanding of the pathophysiological processes that cause AF due in part to the lack of representative models available to elucidate the underlying cellular mechanisms of the arrhythmia. Although atrial-like hiPSC-CMs have been generated to model AF using RA (Devalla et al., 2015; Lee et al., 2017), the calcium handling properties of these cells have not been fully characterized. Using RA-guided differentiation methods we have (1) generated a CM population with an atrial-like molecular and electrophysiologic signature; (2) identified differential regulation of calcium channel genes associated with the RA receptor COUP-TFII; and (3) demonstrated that RA treatment results in modulation of calcium transients and $I_{Ca,L}$. We report for the first time a mechanism by which RA may generate an atrial-like electrophysiologic signature through the downstream regulation of calcium channel gene expression by COUP-TFII and modulation of calcium handling.

Despite the remarkable improvement in efficiency and robustness of protocols for cardiac differentiation of hiPSCs, the resulting CM population is usually a heterogeneous pool of atrial-, nodal-, and ventricular-like cells (Mummery et al., 2012). Native atrial and ventricular CMs exhibit distinct molecular, transcriptomic, and electrophysiologic profiles essential for their diverse physiological roles in the heart, and hiPSC-CM cultures enriched in these subtypes would have significant added value not only in drug response assays but also in elucidating cellular mechanisms of atrial arrhythmias. Here, we directed hiPSCs toward atrial-like CMs by exogenous addition of RA during CM differentiation. RA signaling is crucial for atrial chamber development *in vivo* (Niederreither et al., 2001; Hochgreb et al., 2003), and its activation has previously been shown to steer differentiation of mouse ESCs and hESCs toward atrial-like CMs (Gassanov et al., 2008; Zhang et al., 2011). More recently, it was shown (Lee et al., 2017) that RA signaling at the mesodermal stage of development is necessary for atrial specification and that atrial and ventricular CMs derive from different mesodermal populations. As these may be selected based on RALDH2 and CD235a expression respectively, the generation of highly enriched atrial and ventricular CM populations is highly feasible and will fundamentally accelerate our ability to use them to model AF.

A possible concern for the use of hiPSC-CMs as a modeling system is their relatively immature phenotype. One limitation of our study is that we did not perform a comprehensive electrophysiologic analysis of adult human atrial CMs and therefore cannot rule out the possibility that adult human atrial CMs may exhibit even further functional maturation than atrial-like hiPSC-CMs. However, the calcium handling signature displayed by our atrial-like CMs is similar to that reported for adult human atrial CMs, thus suggesting that hiPSC-derived cells indeed exhibit maturity in terms of calcium handling (Herraiz-Martinez et al., 2015).

Previous studies also report COUP-TFII as a receptor of RA that is involved in the regulation of cardiac potassium channels (Devalla et al., 2015). A more recent report has shown that COUP-TFII can serve as a dual marker for atrial CMs along with NKX2-5, although is not necessary for atrial-like lineage specification (Schwach et al., 2017). Therefore, we postulated that COUP-TFII may function in parallel with lineage specification pathways to modulate selected gene pathways important for the functional maturation of atrial-like cells, such as those involved in the

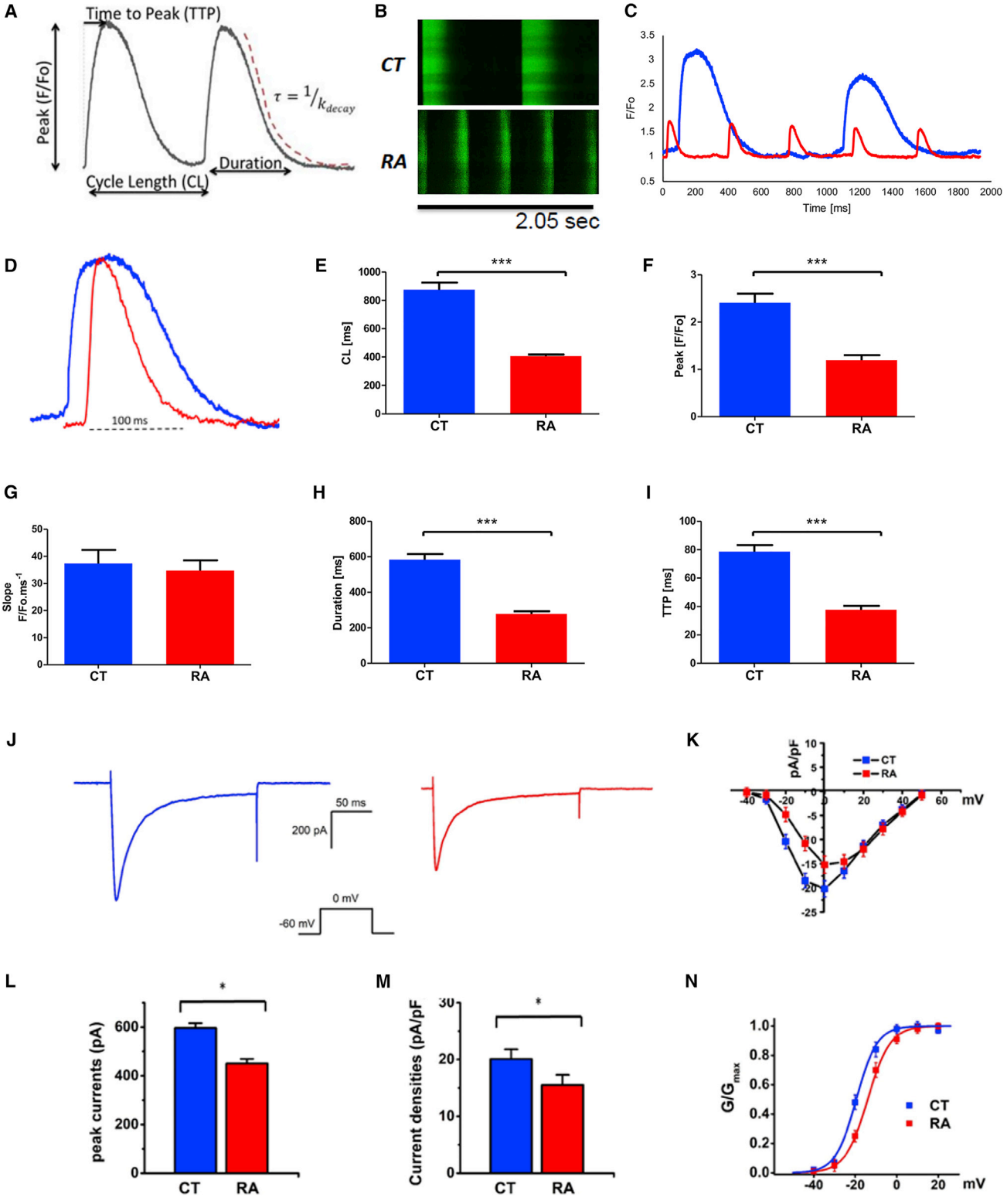

(legend on next page)

regulation of calcium homeostasis. Converging evidence from ENCODE ChIP-seq data and chromatin immunoprecipitation (ChIP)-qPCR results indicate that COUP-TFII interacts with *CACNA1G* and *CACNA1C* and not *NKX2.5* (Figure S2C), implicating a role for COUP-TFII in the direct regulation of *CACNA1G* and *CACNA1C* gene expression and the functional changes observed in atrial-like hiPSC-CM calcium handling.

Genetic approaches to AF have provided important insights into the pathophysiology of the arrhythmia. However, the translation of these discoveries to the bedside care of patients has been limited in part because of incomplete understanding of the underlying cellular mechanisms by which mutations cause AF (Darbar and Roden, 2013). Recent experimental work from our group (Faggioni et al., 2014) and several others (Chelu et al., 2009; Li et al., 2012; Shan et al., 2012) has demonstrated that mutations in either *RyR2* or RyR2 binding proteins that render RyR2 channels "leaky" will make mice susceptible to AF induction. This induction can be prevented by agents that block RyR2 channels, or more specifically reduce RyR2 channel open time (Faggioni et al., 2014; Shan et al., 2012). Collectively, these results indicate that leaky calcium ion channels, such as RyR2, may induce AF and represent an underlying mechanism for the triggering of AF. Thus, improved understanding of calcium handling proteins in atrial-like hiPSC-CMs is important if it is going to be used as an *in vitro* modeling system for AF-linked mutations, especially those involving calcium channels.

CMs have very distinct electrophysiologic properties and heterologous expression systems cannot capture the full spectrum of functional changes associated with AF-linked mutations. A number of reports have used hESCs or hiPSCs to model atrial-specific AADs, cardiac potassium channels, and AF-associated genetic variants (Devalla et al., 2015; Marczenke et al., 2017; Laksman et al., 2017). However, given the important role played by calcium handling proteins in the pathogenesis of AF, this is the first study to fully characterize the calcium handling and identify an electrophysiologic signature for atrial-like hiPSC-CMs. Thus, atrial-like CMs derived from hiPSCs may be useful for modeling AF-linked mutations, especially those related to calcium channels (Shan et al., 2012; Weeke et al., 2014; Tsai et al., 2015), elucidating the underlying cellular mechanisms and assessing mechanism-based therapies. Such an approach will also enable a more "personalized" approach to the treatment of AF. Our findings may also have important implications for drug screening and drug discovery using patient-derived hiPSCs. The development of a high-throughput model for pre-clinical screening of AADs that target atrial-specific cardiac ion channels would prove extremely useful and would be the next step toward personalizing therapy for patients with this common and morbid arrhythmia.

EXPERIMENTAL PROCEDURES

Cell Culture

hiPSC Culture

hiPSC-L1-CMs and hiPSC-L2-CMs were generated, as previously described (Jia et al., 2010), by the Stanford iPSC Biobank and LIMR iPSC Core, respectively. Briefly, three independent clones of each cell line were derived from peripheral blood by lentivirus-based reprogramming. HiPSCs were maintained on human recombinant vitronectin (hrVTN)-coated plates in Essential 8 Flex medium (Gibco). iPSCs were then differentiated using medium A of conditioned CM differentiation kit (Gibco) for 2 days. At day 3, medium is replaced with CM differentiation medium B

Figure 4. RA Treatment of hiPSC-CMs Increases Rate of Calcium Uptake and Release, Reduces L-type Calcium Current, and Limits Channel Availability

(A) Space-averaged calcium transients illustrating the parameters to be analyzed.
(B) Representative line scans showing the sCaREs in CT and RA hiPSC-L1-CMs.
(C) Space-averaged calcium transients comparing spontaneous activity between CT (blue line) and RA (red line) hiPSC-CMs.
(D) Overlap of normalized calcium transients from CT and RA CMs showing differences in TTP, duration, and decay. Comparison of sCaRE parameters from CT- and RA-treated CMs.
(E) Cycle length (CL); n = 25 cells per group.
(F) Peak amplitude; n = 25 cells per group.
(G) Slope; n = 25 cells per group.
(H and I) Duration, n = 25 cells per group (H); TTP, n = 25 cells per group (I).
(J) Representative recordings of the voltage-gated $I_{Ca,L}$ in hiPSC-CMs in CT (left panel) and RA-treated cells (right panel); currents were measured from a holding potential of −90 mV to test potentials ranging from −60 to 0 mV in 10 mV steps; n = 5 cells.
(K) Peak current-voltage relationship (I-V curve) for $I_{Ca,L}$ recorded in hiPCS-CMs treated with RA versus CT cells; n = 5 cells.
(L) Peak current amplitudes; n = 5 cells.
(M) Densities measured at 0 mV; n = 5 cells.
(N) Voltage dependence of activation with a conductance-voltage (G-V curve) for $I_{Ca,L}$ recorded in hiPCS-CMs treated with RA versus CT cells; n = 5 cells.
Data shown in all panels represent pooled independent biological experiments displayed as means ± SD, *p < 0.05, ***p < 0.001.

for 2 days. To guide iPSC-derived CMs into atrial maturation, at day 5, we used an adaptation of the method previously described by Devalla et al. (2015) whereby hiPSC-CMs are treated with 1 μmol/L all-*trans* RA. We treated cells with RA for 5 days with media changes every other day. CT cells were treated with equivalent concentrations of DMSO. At day 10, a low-glucose metabolic selection step was used to enrich CM culture (Sharma et al., 2015).

Immunofluorescence

hiPSCs and hiPSC-CMs were plated in MatTek glass bottom dishes coated with hrVTN and were allowed to grow for 2 days. Cells were fixed for 5 min with ice-cold methanol, permeabilized with PBS + 0.1% Triton X-100 for 10 min at room temperature, and blocked with 1% BSA in PBST (PBS with Tween 20) for 30 min at room temperature. Staining was performed for 1 hr at room temperature using primary antibodies diluted in 1% BSA in PBS. Cells were washed three times with cold PBS and incubated at room temperature for 1 hr with secondary antibodies. Cells were washed three times with PBS and co-stained with 1 μg/mL of DAPI. Samples were imaged using an LSM710 Meta Confocal Microscope (Zeiss). See Supplemental Experimental Procedures for extended description of antibodies.

Flow Cytometry

hiPSCs and hiPSC-CMs were rinsed with Dulbecco's PBS without $CaCl_2$ or $MgCl_2$ (Gibco) and incubated with TrypLE Express (Gibco) for 10 min at 37°C to dissociate the cells. Cells were washed and stained with a fixable live/dead stain (Invitrogen, MP34955) for 30 min to distinguish between live and dead populations. Cells were then fixed with 4% formaldehyde for 10 min and permeabilized with 0.5% Triton X. Cells were incubated and stained with primary antibodies according to manufacturer's instructions. Stained undifferentiated hiPSC-L1 at day 0 served as a negative gating CT for assessing markers of ventricular and atrial differentiation in RA-treated and CT hiPSC-L1-CMs at day 30 of differentiation. See Supplemental Experimental Procedures for extended description on antibodies.

PCR and RNA Sequencing

Cells were harvested and RNA extracted using phenol chloroform extraction. Preparation of cDNA was performed according to manufacturer's instructions using SuperScript IV Reverse Transcriptase (200 U/μL, Invitrogen). The real-time PCR reaction (qPCR) was carried out using FastStart Universal Taqman or SYBR Green Master Mixes (Applied Biosystems). Expression of mRNAs was normalized to the expression of glyceraldehyde 3-phosphate dehydrogenase (GAPDH) mRNA. To obtain the whole transcriptome of the iPSC-CMs, we performed RNA sequencing (RNA-seq) using TempO-Seq (BioSpyder) from cell lysates following manufacturer's instructions. Read counts were analyzed for DEGs among samples. Genes with mean absolute log2 fold change >2 were included in the analysis ($p < 0.05$). Unsupervised hierarchical clustering of all detected genes was performed using the euclidean distance and complete linkage method. Volcano plots were analyzed using R platform. The enriched biological processes were obtained using GO (www.geneontology.org). See Supplemental Experimental Procedures for extended description.

ChIP

ChIP was performed using a ChIP Assay kit (Millipore, Billerica, MA; http://www.millipore.com; catalog no. 17-295) per manufacturer's protocol. Immunoprecipitation was performed using a ChIP-grade COUP-TFII antibody to pull down COUP-TFII: Abcam, Cambridge, UK; http://www.abcam.com; catalog no. ab41859. PCR detection was performed using Applied Biosystems Fast Real-time PCR 7500 system according to manufacturer's instructions with gene-specific primers spanning CACNA1G and CACNA1C binding site regions identified in the encode database.

Ca Measurements

Fluo-4-AM (Molecular Probes) was used to measure changes in Ca concentration. The dye was dissolved in 45 μL of DMSO (Molecular Probes) with 2.5% Pluronic F-127 (Molecular Probes) and added to 1 mL of 1 mM Ca Tyrode's solution. Cells were incubated in 5 μM of Fluo-4-AM for 15 min at room temperature and washed for 15 min with Tyrode's solution containing 2 mM Ca at room temperature before Ca measurements. All experiments were performed using 2 mM Ca concentration. Linescans were registered using an LSM710 Meta Confocal Microscope (Zeiss) and analyzed using ImageJ. See Supplemental Experimental Procedures for extended description.

Cellular Electrophysiology

hiPSC-CMs were differentiated on 35 mm Petri dishes using the protocol described above. Between days 25 and 35, APs were obtained from iPSC-CM monolayers using conventional sharp microelectrode techniques. AP characteristics were obtained during spontaneous beating and also during pacing at the same rate above the spontaneous rate at 2 Hz with the values for AP corrected by frequency using the Bazzet formula. Ventricular, atrial, and nodal APs were classified according to published criteria (Ma et al., 2011). Ventricular-like APs had a ratio (APD30–40/APD70–80) ~1 compared with the atrial-like ratio of ~0.5 and nodal-like ratio of ~0.2. Single-cell patch-clamp measurements were performed in whole-cell configurations using an Axopatch 200B amplifier controlled by pClamp10 software through an Axon Digidata 1440A (Kim et al., 2014). Steady-state activation G-V for Ca currents were fitted by the Boltzmann equation described previously (Pathak et al., 2016). Current densities were calculated by whole-cell current amplitude and capacitance value taken from readings of the amplifier after electronic subtraction of the capacitive transients. See Supplemental Experimental Procedures for extended description.

Statistical Data Analysis

Data are presented as mean ± standard error of the mean (SEM) or mean ± standard deviation (SD) as indicated. For datasets with normal distributions, statistical significance was determined by Student's t test (two-tailed) for two groups or one-way ANOVA for multiple groups with post hoc test Bonferroni.

ACCESSION NUMBERS

The accession number for the RNA sequencing data reported in the paper is GEO: GSE112695.

SUPPLEMENTAL INFORMATION

Supplemental Information includes Supplemental Experimental Procedures, three figures, three tables, and two videos and can be found with this article online at https://doi.org/10.1016/j.stemcr.2018.04.005.

AUTHOR CONTRIBUTIONS

Conception and Experimental Design, M.A., E.L., B.C., J.R., and D.D.; Financial Support, B.C., J.C.W., and D.D.; Collection and Assembly of Data, M.A., E.L., L.H., A.S., M.Z., B.C., A.M., E.S.-G., and D.D.; Data Analysis, M.A., E.L., L.H., B.C., E.S.-G., and D.D.; Manuscript Writing, M.A., E.L., and D.D.; Critical Revisions of the Manuscript, J.R., J.C.W., and D.D.

ACKNOWLEDGMENTS

This work was in part supported by NIH grants R01 HL092217 and HL138737 (D.D.) and R01 HL128170 and R24 HL117756 (J.C.W.).

Received: October 9, 2017
Revised: April 5, 2018
Accepted: April 6, 2018
Published: May 3, 2018

REFERENCES

Chelu, M.G., Sarma, S., Sood, S., Wang, S., van Oort, R.J., Skapura, D.G., Li, N., Santonastasi, M., Muller, F.U., Schmitz, W., et al. (2009). Calmodulin kinase II-mediated sarcoplasmic reticulum Ca2+ leak promotes atrial fibrillation in mice. J. Clin. Invest. *119*, 1940–1951.

Chugh, S.S., Havmoeller, R., Narayanan, K., Singh, D., Rienstra, M., Benjamin, E.J., Gillum, R.F., Kim, Y.H., McAnulty, J.H., Jr., Zheng, Z.J., et al. (2014). Worldwide epidemiology of atrial fibrillation: a Global Burden of Disease 2010 study. Circulation *129*, 837–847.

Darbar, D., and Roden, D.M. (2013). Genetic mechanisms of atrial fibrillation: impact on response to treatment. Nat. Rev. Cardiol. *10*, 317–329.

Devalla, H.D., Schwach, V., Ford, J.W., Milnes, J.T., El-Haou, S., Jackson, C., Gkatzis, K., Elliott, D.A., Chuva de Sousa Lopes, S.M., Mummery, C.L., et al. (2015). Atrial-like cardiomyocytes from human pluripotent stem cells are a robust preclinical model for assessing atrial-selective pharmacology. EMBO Mol. Med. *7*, 394–410.

Faggioni, M., Savio-Galimberti, E., Venkataraman, R., Hwang, H.S., Kannankeril, P.J., Darbar, D., and Knollmann, B.C. (2014). Suppression of spontaneous ca elevations prevents atrial fibrillation in calsequestrin 2-null hearts. Circ. Arrhythm. Electrophysiol. *7*, 313–320.

Gassanov, N., Er, F., Zagidullin, N., Jankowski, M., Gutkowska, J., and Hoppe, U.C. (2008). Retinoid acid-induced effects on atrial and pacemaker cell differentiation and expression of cardiac ion channels. Differentiation *76*, 971–980.

Hatano, S., Yamashita, T., Sekiguchi, A., Iwasaki, Y., Nakazawa, K., Sagara, K., Iinuma, H., Aizawa, T., and Fu, L.T. (2006). Molecular and electrophysiological differences in the L-type Ca2+ channel of the atrium and ventricle of rat hearts. Circ. J. *70*, 610–614.

Herraiz-Martinez, A., Alvarez-Garcia, J., Llach, A., Molina, C.E., Fernandes, J., Ferrero-Gregori, A., Rodriguez, C., Vallmitjana, A., Benitez, R., Padro, J.M., et al. (2015). Ageing is associated with deterioration of calcium homeostasis in isolated human right atrial myocytes. Cardiovasc. Res. *106*, 76–86.

Hochgreb, T., Linhares, V.L., Menezes, D.C., Sampaio, A.C., Yan, C.Y., Cardoso, W.V., Rosenthal, N., and Xavier-Neto, J. (2003). A caudorostral wave of RALDH2 conveys anteroposterior information to the cardiac field. Development *130*, 5363–5374.

Itzhaki, I., Maizels, L., Huber, I., Zwi-Dantsis, L., Caspi, O., Winterstern, A., Feldman, O., Gepstein, A., Arbel, G., Hammerman, H., et al. (2011). Modelling the long QT syndrome with induced pluripotent stem cells. Nature *471*, 225–229.

Itzhaki, I., Maizels, L., Huber, I., Gepstein, A., Arbel, G., Caspi, O., Miller, L., Belhassen, B., Nof, E., Glikson, M., and Gepstein, L. (2012). Modeling of catecholaminergic polymorphic ventricular tachycardia with patient-specific human-induced pluripotent stem cells. J. Am. Coll. Cardiol. *60*, 990–1000.

Jia, F., Wilson, K.D., Sun, N., Gupta, D.M., Huang, M., Li, Z., Panetta, N.J., Chen, Z.Y., Robbins, R.C., Kay, M.A., et al. (2010). A nonviral minicircle vector for deriving human iPS cells. Nat. Methods *7*, 197–199.

Kim, I.H., Hevezi, P., Varga, C., Pathak, M.M., Hong, L., Ta, D., Tran, C.T., Zlotnik, A., Soltesz, I., and Tombola, F. (2014). Evidence for functional diversity between the voltage-gated proton channel Hv1 and its closest related protein HVRP1. PLoS One *9*, e105926.

Laksman, Z., Wauchop, M., Lin, E., Protze, S., Lee, J., Yang, W., Izaddoustdar, F., Shafaattalab, S., Gepstein, L., Tibbits, G.F., et al. (2017). Modeling atrial fibrillation using human embryonic stem cell-derived atrial tissue. Sci. Rep. *7*, 5268.

Landt, S.G., Marinov, G.K., Kundaje, A., Kheradpour, P., Pauli, F., Batzoglou, S., Bernstein, B.E., Bickel, P., Brown, J.B., Cayting, P., et al. (2012). ChIP-seq guidelines and practices of the ENCODE and modENCODE consortia. Genome Res. *22*, 1813–1831.

Lee, J.H., Protze, S.I., Laksman, Z., Backx, P.H., and Keller, G.M. (2017). Human pluripotent stem cell-derived atrial and ventricular cardiomyocytes develop from distinct mesoderm populations. Cell Stem Cell *21*, 179–194.e4.

Li, N., Wang, T., Wang, W., Cutler, M.J., Wang, Q., Voigt, N., Rosenbaum, D.S., Dobrev, D., and Wehrens, X.H. (2012). Inhibition of CaMKII phosphorylation of RyR2 prevents induction of atrial fibrillation in FKBP12.6 knockout mice. Circ. Res. *110*, 465–470.

Liang, G., and Zhang, Y. (2013). Embryonic stem cell and induced pluripotent stem cell: an epigenetic perspective. Cell Res. *23*, 49–69.

Liang, P., Sallam, K., Wu, H., Li, Y., Itzhaki, I., Garg, P., Zhang, Y., Vermglinchan, V., Lan, F., Gu, M., et al. (2016). Patient-specific and genome-edited induced pluripotent stem cell-derived cardiomyocytes elucidate single-cell phenotype of Brugada syndrome. J. Am. Coll. Cardiol. *68*, 2086–2096.

Ma, J., Guo, L., Fiene, S.J., Anson, B.D., Thomson, J.A., Kamp, T.J., Kolaja, K.L., Swanson, B.J., and January, C.T. (2011). High purity

human-induced pluripotent stem cell-derived cardiomyocytes: electrophysiological properties of action potentials and ionic currents. Am. J. Physiol. Heart Circ. Physiol. *301*, H2006–H2017.

Marczenke, M., Piccini, I., Mengarelli, I., Fell, J., Ropke, A., Seebohm, G., Verkerk, A.O., and Greber, B. (2017). Cardiac subtype-specific modeling of Kv1.5 ion channel deficiency using human pluripotent stem cells. Front. Physiol. *8*, 469.

Mummery, C.L., Zhang, J., Ng, E.S., Elliott, D.A., Elefanty, A.G., and Kamp, T.J. (2012). Differentiation of human embryonic stem cells and induced pluripotent stem cells to cardiomyocytes: a methods overview. Circ. Res. *111*, 344–358.

Niederreither, K., Vermot, J., Messaddeq, N., Schuhbaur, B., Chambon, P., and Dolle, P. (2001). Embryonic retinoic acid synthesis is essential for heart morphogenesis in the mouse. Development *128*, 1019–1031.

Patel, N.J., Deshmukh, A., Pant, S., Singh, V., Patel, N., Arora, S., Shah, N., Chothani, A., Savani, G.T., Mehta, K., et al. (2014). Contemporary trends of hospitalization for atrial fibrillation in the United States, 2000 through 2010: implications for healthcare planning. Circulation *129*, 2371–2379.

Pathak, M.M., Tran, T., Hong, L., Joos, B., Morris, C.E., and Tombola, F. (2016). The Hv1 proton channel responds to mechanical stimuli. J. Gen. Physiol. *148*, 405–418.

Pereira, F.A., Qiu, Y., Zhou, G., Tsai, M.J., and Tsai, S.Y. (1999). The orphan nuclear receptor COUP-TFII is required for angiogenesis and heart development. Genes Dev. *13*, 1037–1049.

Schwach, V., Verkerk, A.O., Mol, M., Monshouwer-Kloots, J.J., Devalla, H.D., Orlova, V.V., Anastassiadis, K., Mummery, C.L., Davis, R.P., and Passier, R. (2017). A COUP-TFII human embryonic stem cell reporter line to identify and select atrial cardiomyocytes. Stem Cell Reports *9*, 1765–1779.

Shan, J., Xie, W., Betzenhauser, M., Reiken, S., Chen, B.X., Wronska, A., and Marks, A.R. (2012). Calcium leak through ryanodine receptors leads to atrial fibrillation in 3 mouse models of catecholaminergic polymorphic ventricular tachycardia. Circ. Res. *111*, 708–717.

Sharma, A., Li, G., Rajarajan, K., Hamaguchi, R., Burridge, P.W., and Wu, S.M. (2015). Derivation of highly purified cardiomyocytes from human induced pluripotent stem cells using small molecule-modulated differentiation and subsequent glucose starvation. J. Vis. Exp. https://doi.org/10.3791/52628.

Shi, Y., Inoue, H., Wu, J.C., and Yamanaka, S. (2017). Induced pluripotent stem cell technology: a decade of progress. Nat. Rev. Drug Discov. *16*, 115–130.

Tsai, C.T., Hsieh, C.S., Chang, S.N., Chuang, E.Y., Juang, J.M., Lin, L.Y., Lai, L.P., Hwang, J.J., Chiang, F.T., and Lin, J.L. (2015). Next-generation sequencing of nine atrial fibrillation candidate genes identified novel de novo mutations in patients with extreme trait of atrial fibrillation. J. Med. Genet. *52*, 28–36.

Weeke, P., Muhammad, R., Delaney, J.T., Shaffer, C., Mosley, J.D., Blair, M., Short, L., Stubblefield, T., Roden, D.M., and Darbar, D. (2014). Whole-exome sequencing in familial atrial fibrillation. Eur. Heart J. *35*, 2477–2483.

Zhang, Q., Jiang, J., Han, P., Yuan, Q., Zhang, J., Zhang, X., Xu, Y., Cao, H., Meng, Q., Chen, L., et al. (2011). Direct differentiation of atrial and ventricular myocytes from human embryonic stem cells by alternating retinoid signals. Cell Res. *21*, 579–587.